arXiv:1407.5034v2 [cond-mat.mes-hall] 29 Jul 2014

Quantitative μPIV Measurements of Velocity Profiles

Bryant, P. W.[1,†], Neumann, R. F.[1,†], Moura, M. J. B.[1,†], Steiner, M.[1], Carvalho, M. S.[2], and Feger, C.[1]

[1]IBM Research – Brazil, Av. Pasteur 138 & 146, Urca, Rio de Janeiro, CEP 22290-240, Brazil

[2]Dept. Mech. Eng., PUC–Rio, R. Marquês de São Vicente, 225, Gávea, Rio de Janeiro, Brazil

[†]Equal contribution

July 31, 2014

Abstract

In Microscopic Particle Image Velocimetry (μPIV), velocity fields in microchannels are sampled over finite volumes within which the velocity fields themselves may vary significantly. In the past, this has limited measurements often to be only qualitative in nature, blind to velocity magnitudes. In the pursuit of quantitatively useful results, one has treated the effects of the finite volume as errors that must be corrected by means of ever more complicated processing techniques. Resulting measurements have limited robustness and require convoluted efforts to understand measurement uncertainties. To increase the simplicity and utility of μPIV measurements, we introduce a straightforward method, based directly on measurement, by which one can determine the size and shape of the volume over which moving fluids are sampled. By comparing measurements with simulation, we verify that this method enables quantitative measurement of velocity profiles across entire channels, as well as an understanding of experimental uncertainties. We show how the method permits measurement of an unknown flow rate through a channel of known geometry. We demonstrate the method to be robust against common sources of experimental uncertainty. We also apply the theory to model the technique of Scanning μPIV, which is often used to locate the center of a channel, and we show how and why it can in fact misidentify the center. The results have general implications for research and development that requires reliable, quantitative measurement of fluid flow on the micrometer scale and below.

1 Introduction

Microscopic Particle Image Velocimetry (μPIV) has become an invaluable measurement technique for probing fluid flow in systems at the micro- and the nano-scale [1, 2, 3, 4]. Well-

controlled and understood μPIV experiments performed on increasingly complex systems will become crucial to maintaining the rapid progress observed in the biomedical and natural resources industries [5, 6, 7]. When imaging only over a region small compared to the size of a microfluidic system, it is sometimes possible optically to restrict the volume over which the system is probed. The result is often a quantitative measurement of fluid flow in that region [8, 9]. To image simultaneously as many flow features as possible, however, one requires a field of view of size comparable to the length scales of the system. Unfortunately, this leads inevitably to having also a large depth of field along the optical axis, which is an issue [10, 11, 12] that hinders a straightforward quantification and interpretation of results. For μPIV to reach its full potential as an investigative and design tool, it must provide repeatable and quantitatively useful results. It has been an open question whether or not this is possible for μPIV with a depth of field of size comparable to that of the microfluidics system it measures.

There are two standard approaches to treating the effects of a large depth of field. The first is to limit μPIV to qualitative comparisons of velocity profile shapes, often away from channel walls. In such cases, one treats the volumetric flow rate of the fluid as a free parameter used to match expected profiles to the measured data [10, 11]. In the second approach, one treats finite volume effects as measurement errors, particularly near the walls, and attempts to remove as many of these effects as possible via data processing. This approach has, to some extent, enabled the quantitative evaluation of μPIV data [12, 13, 14, 15].

A shortcoming of the latter method, however, is the often complicated and convoluted data processing that limits or even precludes the physical understanding of the fluid flow and its analysis. It bears the risk of over-fitting results to the extent that important flow features are missed, or even misdiagnosing the causes of observed phenomena. An example is the spurious, increasing velocity near the channel walls that sometimes appears [13, 15]. In most cases noisy or uncertain experimental data are excluded from the measured flow profile altogether, without physical justification. A related problem is that excessive data processing introduces additional sources of experimental uncertainty in an obscure fashion.

In this article, we investigate the results of a series of experiments performed with a large depth of field μPIV, in which we image across the entire microchannel and measure the velocity profile from wall to wall. Rather than use data processing to remove the effects of finite measurement volumes, we introduce the concept of Sampling Volume (SV) over which the velocity field can be averaged to recover the measured velocity profiles. We then systematically determine the size and shape of the SV using an error minimization procedure. For our experiment, which is described below, we find that measurements near the walls reflect in a straightforward manner the non-trivial intersection of the SV with the edges of the microchannel. Consequently, the entire measured profile contains information useful for determining the SV, and one should therefore not discard features measured near channel walls.

We begin with a discussion of μPIV for large depth of field and a motivation for our definition of the SV. We then describe our experimental setup and how our data are processed

and analyzed. We also discuss the expected velocity field in the channel, and its relevant sources of uncertainty. Then we show how averaging the velocity field over a rectangular SV reproduces to within our experimental uncertainty the measured velocity profiles across the entire channel. We also demonstrate how, because of the simplicity of our method and the minimal post-processing of data, μPIV can in some cases be used to infer an unknown velocity field or flow rate in a channel of known cross section. We close with a series of use cases for our approach, which include robustly measuring velocity profiles in the presence of camera misalignment and very noisy data that would typically be deemed useless, a demonstration of how data processing affects the SV, and finally a critical analysis of the procedure known as "Scanning PIV," which is often used to place a measurement domain at the center of microchannels [12, 16]. We show why, for finite-sized SV, Scanning PIV does not necessarily locate the center of a microchannel, and should therefore be used with caution.

2 Particle Image Velocimetry

2.1 General description

Particle Image Velocimetry (PIV) is an optical method for visualizing and measuring flow fields. One seeds a fluid with tracer particles, and if the particles follow the fluid flow without disturbing it significantly, by analyzing their trajectories one can infer the velocity field of the moving fluid. To determine the particle displacements one uses consecutive snapshots of the system taken at times t and $t + \Delta t$, containing several particle images at various positions. The snapshots are subdivided into smaller regions called "interrogation windows" and the net particle displacement is calculated for each one of them. Finally, the velocity representative of each window is calculated simply by dividing the respective displacement by the interval, Δt, between frames.

Analyzing and interpreting a PIV measurement is complicated for the following reasons. First, the velocity obtained from this process is an average in space and time, and its accuracy depends on the flow field itself, as well as on both spatial and temporal resolution of the experimental setup [17]. Second, tracer particles are susceptible to Brownian motion, and as a consequence their positions in images must be correlated within sub-ensembles to suppress the effect of random movements and determine net particle displacements. The application of cross-correlation techniques ultimately provides a 2D projection of the 3D velocity field of the fluid located within the imaged region, as viewed from the camera [4].

In Microscopic PIV (μPIV), see Figure 1(a), fluorescent tracer particles in a fluid channel of arbitrary geometry are observed by means of an optical microscope setup. The size of the tracer particles needs to be chosen carefully such that particles emit a sufficient amount of light for detection without perturbing the flow. To perform the measurement, one focuses a laser pulse on the fluid channel to excite the tracer particles. The particles then emit light at a red-shifted fluorescence wavelength that is collected by the same objective lens, alongside with the reflected laser light. The reflected excitation laser light is then filtered out by a dichroic beam splitter while the fluoresced light passes, rendering fluorescence images

of spatially resolved particles on the CCD array. As indicated in Figure 1(a), fluorescent particles (red) in the object plane are spatially resolved in the conjugate image plane with a lateral resolution in x and y that is determined by the specifics of the optical setup. However, a particle's image will only be detectable if its z-position falls within the finite range labeled δ in Figure 1(b), which depends not only on the characteristics of the optical setup but also on the data processing algorithms used in the analysis. In the following section, we will introduce a concept for the determination of the volume probed by a μPIV experiment.

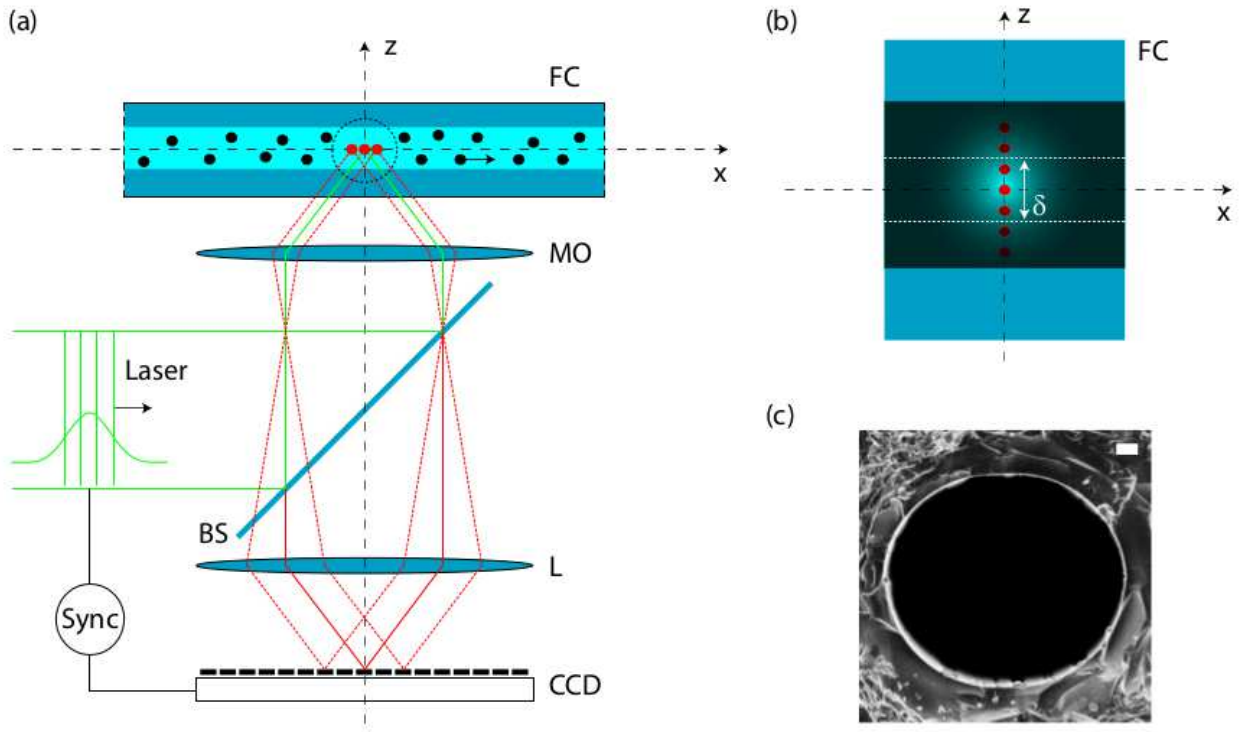

Figure 1: (a) Simplified schematic of the μPIV setup. The flow direction of fluorescent particles in the fluidic channel (FC) is indicated by an arrow. MO: microscope objective; BS: dichroic beam splitter; L: lens; CCD: charge coupled device array detector. (b) Schematic of the fluidic channel showing the depth of the SV, δ. (c) Scanning electron microscope image of the cross section of the fluid channel used in the flow experiments. The length of the white scale bar represents 10 μm.

2.2 Sampling Volume

In this paper, our main concern is a well-known complication inherent to μPIV with a large depth of field, for which tracer particles are imaged over a finite volume with a characteristic length scale on the order of the scale of the microchannels themselves. Besides the well established *depth of field* and *depth of focus* [4, 18], several other quantities have been used to quantify the depth over which the system is probed. Among them are the laser

light sheet [4, 10], the depth of measurement [19], and the depth of correlation [11, 12, 20]. Although they have various meanings and account for various effects, many of them derive from the basic definition of the depth of field.

The term "laser light sheet" [4, 10] was introduced to denote the illuminated region inside the fluid system. In most μPIV applications the light sheet and the entire fluid system are of comparable sizes. When that is the case, all particles inside the channel are excited by the laser light and, in general, all fluorescent particles within the (x, y) field of view of the optical setup and within the depth of field, Δz, create in-focus images on the CCD detector. The geometrical shape of this volume can be approximated as a parallelepiped, and the focal (x, y)-plane oriented perpendicular to the optical z axis cuts this volume in half.

In standard far-field fluorescence microscopy the total point spread function and, hence, the size of the focal volume is determined by the product of the excitation point spread function and the detection point spread function [18]. In μPIV, however, where image processing is used to determine the particles' displacements over successive frames, there are additional contributions that alter the effective volume that is being probed, such as the application of the image pair correlation function [21]. As a consequence, a "depth of correlation" (DOC) was introduced to estimate the depth of the volume that contains those particles contributing significantly to the spatial correlation function [11, 12, 20]. The calculated DOC is useful for identifying the experimental parameters relevant to the probed volume. However, it is based on an assumed intensity threshold beyond which imaged particles do not "cause a significant bias in the velocity estimate" [15]. It is thus not quantitatively well defined, and has not led to conclusive results in comparison with experiments [11, 12]. In Section 6.3 we will present a series of results that indicate the DOC should be used only as an order-of-magnitude estimate of the probed volume.

Despite significant effort to determine precisely the probed volume, a simultaneously intuitive and quantitative definition is lacking. To address this issue, we introduce a quantity with a straightforward and verifiable interpretation. We call it Sampling Volume (SV), and it is designed to account for the combined effects of illumination scheme, optical depth, and image processing. The concept, as opposed to previously defined quantities such as the DOC, is strikingly simple: the SV is defined as the volume over which one averages the velocity field of the fluid in order to recover the measured profile.

We begin with a complete description of our averaging process for one experiment performed on a simple, straight channel, for which we will ignore any variation in measured velocity down the channel (x direction). We denote the velocity field within the channel by $\vec{v}(x, y, z)$. Because of the translational symmetry in x, we take $\vec{v}(x, y, z) \to \vec{v}(y, z)$. The velocity averaged over the SV, which is compared with measurements, is then

$$\langle \vec{v} \rangle_{SV}(y) = \frac{\int_{z_-(y)}^{z_+(y)} dz\, \vec{v}(y, z)}{z_+(y) - z_-(y)}, \tag{1}$$

as a function of y, which is the direction across the channel, as seen below in Figure 3. In (1),

the integration bounds for a rectangular SV are defined by

$$z_{-} \equiv \mathrm{Max}\left(c - \frac{\delta}{2}, z_{\mathrm{bot}}(y)\right) \tag{2}$$

and

$$z_{+} \equiv \mathrm{Min}\left(c + \frac{\delta}{2}, z_{\mathrm{top}}(y)\right). \tag{3}$$

In (2) and (3), $\mathrm{Max}(\cdot)$ and $\mathrm{Min}(\cdot)$ denote the maximum and minimum values of the arguments. The bottom and top locations of the channel itself are $z_{\mathrm{bot}}(y)$ and $z_{\mathrm{top}}(y)$, respectively. The vertical center of the SV, as measured with respect to the channel center, is denoted by c, and the vertical depth, or thickness, of the SV is represented by δ. The selection of the maximum or minimum values in the integration bounds is necessary to keep from continuing the average beyond the channel's extent, where no fluid exists. In Section 6.4 is a demonstration of how failing to cut off the average properly at the edge of the channel can lead to a calculated velocity of limited applicability. Throughout Sections 4 and 6 are several demonstrations of the success of using Equation (1) to explain measurements.

3 Experimental Methods and Data Analysis

3.1 Flow Field Measurements

In this section, we briefly describe the experimental setup used for performing all the fluid flow experiments discussed in this article. Further description of the experimental setup can be found in Ref. [22]. The experiments were performed using a commercially available μPIV system (TSI Inc.), composed of an optical microscope, CCD camera, two lasers, and a laser pulse synchronizer. The system is operated by a data acquisition and management software (Insight 3G, TSI Inc.). The inverted microscope (IX71S1F-3, Olympus) is equipped with a 10x/0.30 air objective (UPlanFL N, Olympus). The Peltier-cooled CCD (Sensicam 630166, PowerView) has a resolution of 1376×1024 pixels (1.4MP) and a 2x projection lens. The two pulsed Nd:YAG lasers (Gemini PIV-15, NEW WAVE) operate at 532 nm and a frequency of 15 Hz, providing a pulse energy of 50 mJ. From the specifications of the optical setup we can calculate our depth of field [18] to be approximately $20\,\mu$m. The laser pulse synchronizer (610034, TSI Inc.) controls the timing sequence of laser pulses and exposure time of the CCD. For each flow experiment, 100 pairs of images were collected with a time interval, Δt, of $500\,\mu$s between successive images.

A glass microfluidic device manufactured by Dolomite Centre Ltd, UK was used to perform the flow experiments. The device has a straight channel with an elliptical cross-section, with a semi-minor axis of $50\,\mu$m and semi-major axis of $55\,\mu$m. To visualize the flow we use a mix of 14% aqueous solution of fluorescent particles of $1\,\mu$m in diameter (ex/em 542/612 nm, Thermo Scientific Fluoro-Max Dyed Red Aqueous Fluorescent Particles) and 86% purified water (Thermo Scientific Nalgene Analytical Filter, $0.2\,\mu$m). This fluid mix is injected in the device with the use of a syringe pump (11 Elite syringe pump 704501, Harvard Apparatus). The injection rates ranged from $75\,\mu$l/h to $100\,\mu$l/h.

3.2 Measurement Uncertainty

The extent to which we can determine the size and shape of our SV depends on our experimental uncertainties, as will be demonstrated in Sections 4 and 6. We therefore performed several calibration procedures to assess the accuracy and precision of our measurements.

The major sources of uncertainty in the fluid flow itself are in the microchannel geometry and the flow rate provided by the syringe pump. With a scanning electron microscope, we imaged representative cross sections of our channels. Figure 1 contains a sample image. We digitized the boundary from two separate images and found that all digitized points lie within the region between two ellipses with semi-major and semi-minor axes of $(55 \pm 1.5)\,\mu$m and $(50 \pm 1.5)\,\mu$m, respectively. The syringe pump was calibrated by measuring the amount of fluid injected over time. Five measurements were taken for each of three injection rates. The measurements were also compared with the total infused volume and the time elapsed, as given on the pump's display. We obtained a 3% uncertainty in the volumetric flow rate, which is consistent with the uncertainty of 0.5% provided by the manufacturer. For our results in Sections 4 and 6, we assume an uncertainty of 0.5% of the flow rate. We also tested the syringe pump connected to the microfluidic system to check for internal pressure effects. Again we measured the infused volume over time. No significant change in the injection rates was observed.

To address the uncertainty in lengths measured by the μPIV system, we calibrated the camera's field of view using a standard calibration target. For our experimental setup the field of view is $(440\pm5)\,\mu\text{m} \times (325\pm5)\,\mu$m, in agreement with the equipment's specifications.

3.3 Data Processing

Image processing of the results presented in Section 4 was carried out using the Insight 3G software, starting from the raw images. We used an interrogation window of 32×32 pixels, with a 50% overlap according to the Nyquist sampling criterion. The FFT correlator and the 3-point Gaussian peak detection were employed in the determination of particle displacements. In order to increase the signal-to-noise ratio, we subtracted background noise and performed an ensemble average over correlation functions across 100 pairs of snapshots. From the camera's pixel resolution and the field of view we know that one pixel corresponds to $0.32\,\mu$m in both the x and the y direction. The overall resolution is therefore $5.12\,\mu$m. With this resolution we obtain 85 velocity vectors along the channel length and 21 along the channel width. Because of the low Reynolds number, the resulting flow is as expected laminar and stable. Figure 2(a) shows a typical velocity profile, which will be further analyzed in Sec. 4.

Velocity profiles were also obtained independently starting from the same raw images and analyzing them with the OpenPIV [23] software [1]. The processing options for OpenPIV, such as the geometry of the interrogation windows, the cross-correlation method, and the peak detection algorithm, were the same as those employed by Insight 3G. The difference was in the noise reduction algorithms: instead of performing an ensemble average over correlation

[1] `http://www.openpiv.net`

functions, we averaged the flow field themselves over the 100 pairs of snapshots, and we did not perform background noise subtraction. The results of the two processing methods are discussed in Section 6.3.

(a)

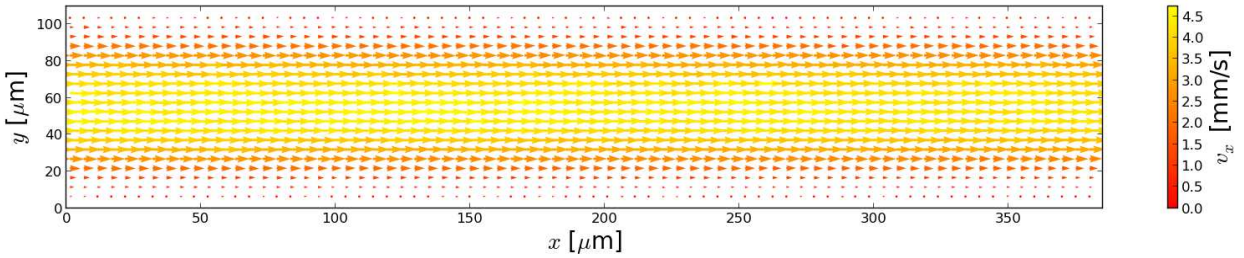

(b)

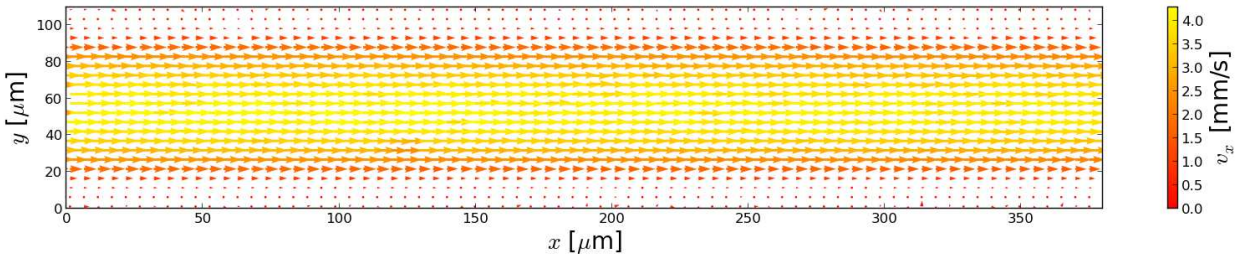

Figure 2: Quiver plots of the measured velocity field as processed by (a) Insight 3G and (b) OpenPIV.

4 Results

For comparison with theory we averaged the profiles located along the (streamwise) x direction. The resulting average profile for an injection rate of $100\,\mu$l/h is pictured in Figure 3(a) as dots with vertical error bars corresponding to one standard deviation. Horizontal error bars representing the uncertainty in length calibration discussed in Section 3.2 are too small to be seen. The large speeds with large error bars beyond the channel walls are numerical artifacts from data processing.

We used Equation (1) to calculate $\langle v \rangle_{SV}(y)$ for a given thickness, δ, and position, c, of the SV. To compute the velocity field, $\vec{v}(x, y, z)$, we used the Lattice Boltzmann Method [24], to which is input the injection rate of the pump, the channel geometry, and the fluid properties. To determine the position, c, and the thickness, δ, of the SV that results in the measured profile, we searched for possible fits to the data by varying c and δ while keeping $\vec{v}(x, y, z)$ fixed. In other words, we did not vary the pressure drop or the injection flow rate, and thus the magnitude of the theoretically expected velocity field is not a free parameter. In

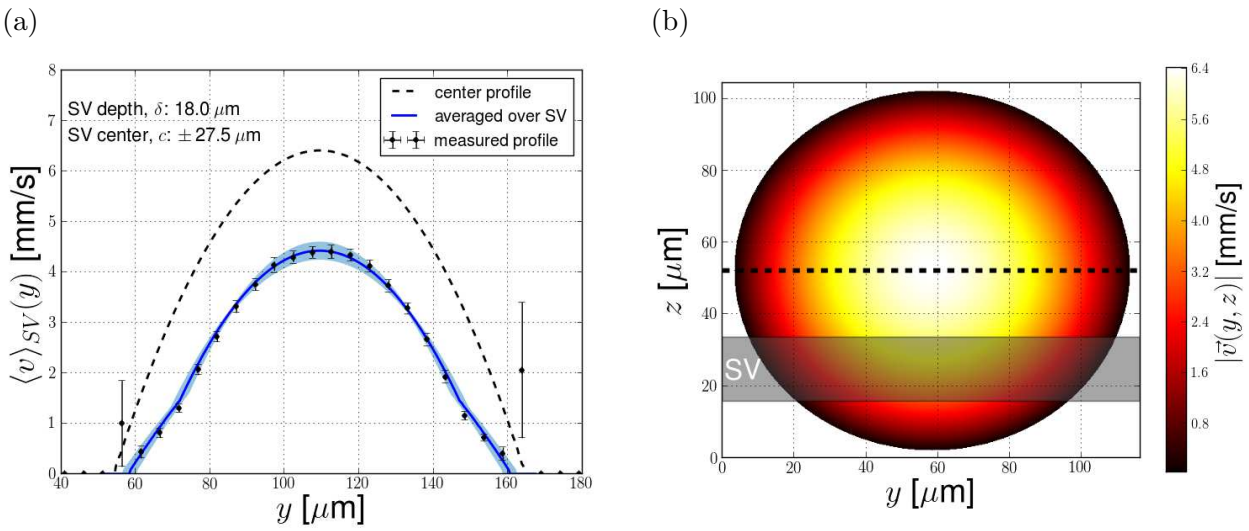

Figure 3: (a) Measured and theoretically expected velocity profiles for an injection rate of $100\,\mu$l/h. (b) The magnitude of the simulated velocity field, $|\vec{v}(y,z)|$, is overlaid by the SV (shaded rectangle) that results in the fit. The dashed line in both images corresponds to a centered SV of zero thickness.

Figure 3(a), the solid blue line is $\langle v\rangle_{SV}(y)$ calculated for an elliptical channel with semi-major and semi-minor axes of $55\,\mu$m and $50\,\mu$m, respectively, and a flow rate delivered by the pump of $100\,\mu$l/h. The shaded area represents the combined effect of the uncertainty in the channel shape and the flow rate, as discussed in Section 3.2. The dashed line, included for reference, is the calculated velocity profile at the center of the channel, $c = 0$.

The fit in Figure 3 is for $\delta = 18\,\mu$m and $c = \pm 27.5\,\mu$m. The position can be positive or negative because the channel has a reflection symmetry with respect to a horizontal plane bisecting it. The lower location is depicted in Figure 3(b). These two parameters that determine the disposition of the SV were found by sweeping through a range of values, for which Figure 4 shows the residual, ϵ. It is clear that no other choices for the center and depth of a rectangular SV can fit the data as well.

Based on this fit, we conclude that, to within our experimental uncertainty, for this test there is a rectangular SV over which one can average the velocity field to match the measured velocity profile. The result is a quantitatively useful μPIV measurement of a velocity profile across the entire width of a channel. In Section 6 are several more examples of successful fits to experimental results. It has been claimed recently [12], however, that the simple average over a sampling region cannot reproduce velocity profiles obtained by μPIV with a large depth of field. Our analysis in Section 6.4 indicates that this claim may result from the incorrect use of a technique called Scanning PIV to locate the vertical center of a channel.

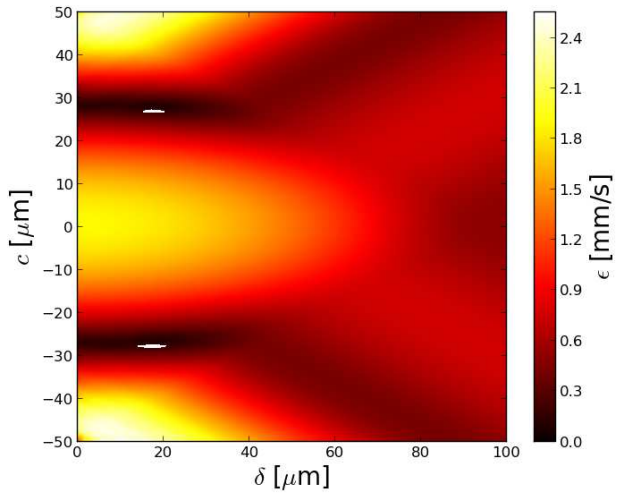

Figure 4: Dependence of the residual, ϵ, with respect to the fit parameters c (the SV center) and δ (the SV thickness). The white spots around the minima depict regions in which ϵ is no more than 20% larger than its lowest value.

5 Inferring Flow Rate, Channel Geometry, or Velocity Field

In Section 4, we demonstrated how to determine the SV for a system in which the flow rate, channel geometry, and fluid properties are known. An important benefit of minimizing the post-processing of data and instead working with the SV is that one may be able to reverse the analysis and infer either the flow rate, the velocity field, or the channel geometry in systems where one of them is not known. For example, a common approach when one uses μPIV to measure the flow rate of, for example, blood in an artery or oil in porous media [7], is to measure the velocity profile and then match the maximum velocity to the peak of the theoretically expected profile, such as the Hagen-Poiseuille profile for cylindrical channels. As is clear from our analysis of the SV, however, this approach will underestimate the experimental flow rate.

One can already obtain a better evaluation from the same data by acknowledging the presence of the SV. If one first calibrates the μPIV apparatus for a well-controlled experiment in which the thickness, δ, of the SV is determined for a given set of optical and processing parameters, as described in Section 4, one can use the knowledge of δ to understand the degree to which a measured velocity profile will underestimate the actual flow rate.

Perhaps more interestingly, by retaining all measured features, such as the kinks near the walls in the profiles seen in Figure 3(a), for some channel shapes one can determine with a single experiment the size and position of the SV, without fitting $\langle v \rangle_{SV}(y)$ to the measured profile. As shown in Figure 5 for our experiment, the y values where the measured profile goes to zero uniquely determine where the top of the SV intersects the channel's walls, where

the velocity field itself is zero. Similarly, the profile's kinks determine where the bottom of the SV intersects the walls. With c and δ uniquely determined, and given the measured velocity magnitudes, one can infer the flow rate or even the velocity field of the flowing fluid. For example, if we had known the channel geometry but not the flow rate for the measurement described above, we could have recovered, to within experimental uncertainty, the entire velocity field by performing several simulations with various flow rates.

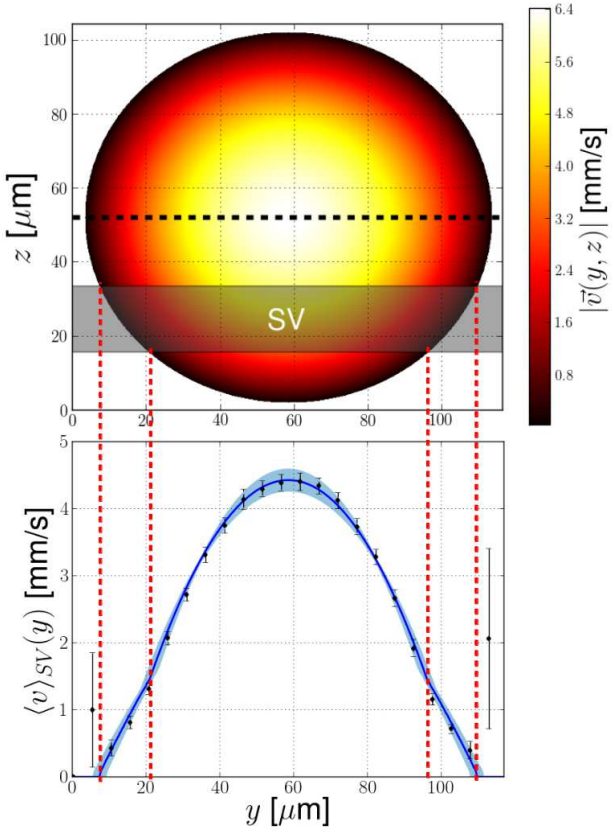

Figure 5: Correspondence between the intersections of the channel walls with the SV and the position of the near-wall features.

In this scenario, one must know the fluid properties and have enough knowledge of possible flow rates to choose correctly the μPIV parameters such as the Δt between images. For some channel shapes and SV sizes, a unique determination of c and δ may not be possible from a single measured profile. In that case, the theory can still be used to identify a set of possible solutions and to judge the relative likelihood of the possibilities. Furthermore, by parallel reasoning, one can reverse the process: If one knows the flow rate but not the channel geometry, one can in principle iterate over possible channel shapes to infer as much as possible about the unknown geometry of the microchannel itself.

Another intriguing possibility is to verify flow models for complex fluids that present non-Newtonian behavior, for which theoretical models or numerical solutions may not be

accurate. In this case, one must either determine the SV as in Figure 5, or else by means of a calibration experiment using known optical parameters and a well-understood fluid, such as we have described in Section 4. Then one can measure the velocity profile of the complex fluid, and the result will be a μPIV measurement that can provide quantitative insight into the various theoretical treatments of the complex fluid.

6 Use Cases

Here we describe several use cases for the simple theory of the SV presented in Section 4. These use cases demonstrate its robustness against common sources of experimental error and against noisy data, its utility for quantifying the effect of processing variables, and how the theory has led to a deeper understanding of the Scanning PIV technique.

6.1 Robustness Against Camera Misalignment

In some experiments, we measured a consistent and smooth drop in the velocity along the x direction, which is the direction of flow. One example can be seen in Figure 6, for the speed at the center (in y) of the channel as it changes in the x direction. Once an experiment was prepared and fluid was flowing, the change in velocity down the channel was consistent, even for other locations along the length of the channel. In other experiments, such as the one presented in Figure 3, there was no appreciable change in velocity down the channel. The simplest explanation for this occasional smooth change in velocity is an occasional misalignment between the camera and the microchannel.

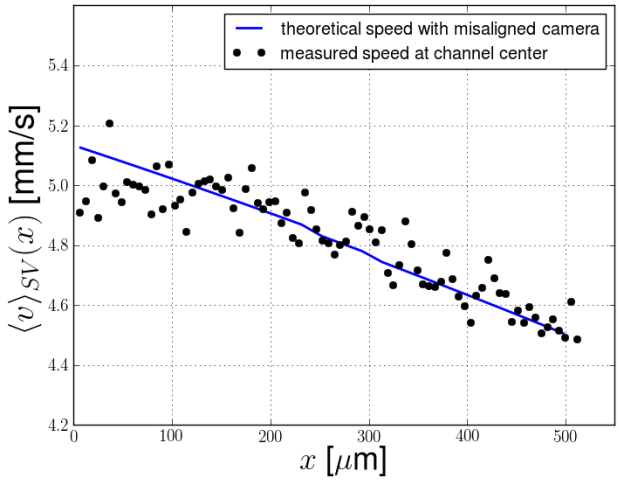

Figure 6: The points represent the speed measured at the center of the cross section for several positions along x, the direction of flow. The solid line shows the theoretically expected speed, $\langle v \rangle_{SV}(x, y = y_{\text{center}}) \equiv \langle v \rangle_{SV}(x)$ calculated at the center of the profile using Equations (4), (5), and (6).

With our method, one can easily treat a misaligned camera. The translational symmetry of the channel is unaffected, so we continue to use $\vec{v}(x,y,z) \rightarrow \vec{v}(y,z)$ for the velocity field inside the channel. The position and shape of the SV do depend on the optical system, however, so we model a misalignment of the camera by varying in x the position of the center of the SV: $c \rightarrow c(x)$. The result is an expected measured velocity that also varies in x, $\langle \vec{v} \rangle_{SV}(x,y)$, which is calculated as

$$\langle \vec{v} \rangle_{SV}(x,y) = \frac{\int_{z_-(x,y)}^{z_+(x,y)} dz\, \vec{v}(y,z)}{z_+(x,y) - z_-(x,y)}. \tag{4}$$

Here the integration bounds must be defined as

$$z_-(x,y) \equiv \mathrm{Max}\left(c(x) - \frac{\delta}{2}, z_{\mathrm{bot}}(y) \right) \tag{5}$$

and

$$z_+(x,y) \equiv \mathrm{Min}\left(c(x) + \frac{\delta}{2}, z_{\mathrm{top}}(y) \right). \tag{6}$$

For the fit in Figure 6 the thickness of the SV, δ, is a constant $18\,\mu$m. The center of the SV, $c(x)$, varies linearly from $c(x = 6\,\mu\mathrm{m}) = -21.7\,\mu$m to $c(x = 517\,\mu\mathrm{m}) = -27\,\mu$m. The channel depth is $100\,\mu$m, so the fit in Figure 6 suggests a camera misalignment of approximately 0.6°, which is reasonable for our experimental setup. Even though the camera was misaligned, we were able to verify the flow in the microchannel.

6.2 Robustness Against Noisy Data

In the past, when normalized velocities have been measured in a more qualitative fashion [10, 11], interesting features in velocity profiles, such as the kinks highlighted in Figure 5, have typically been ignored. In the more quantitative evaluations [12, 14, 15], one has tried to eliminate any kinks or other features near walls via post-processing meant to reduce the effects of a finite SV.

With Figure 7 we demonstrate how maintaining such features can in fact lead to more robust μPIV measurements, particularly when one has noisy data. In this experiment, raw particle images included a large, stationary bright spot that resulted, after processing, in the area with zero velocity shown in Figure 7(a). The average profile, shown in Figure 7(b), has large uncertainty in the center of the channel. Rather than discard the results of the experiment, by fitting the entire measured speed profile, from wall to wall, we were able to quantify the flow in the microchannel. Because we fit the entire profile, and thereby incorporate more data that have been minimally processed, we believe that quantitative evaluation using the SV is significantly more robust and more straightforward than with other methods.

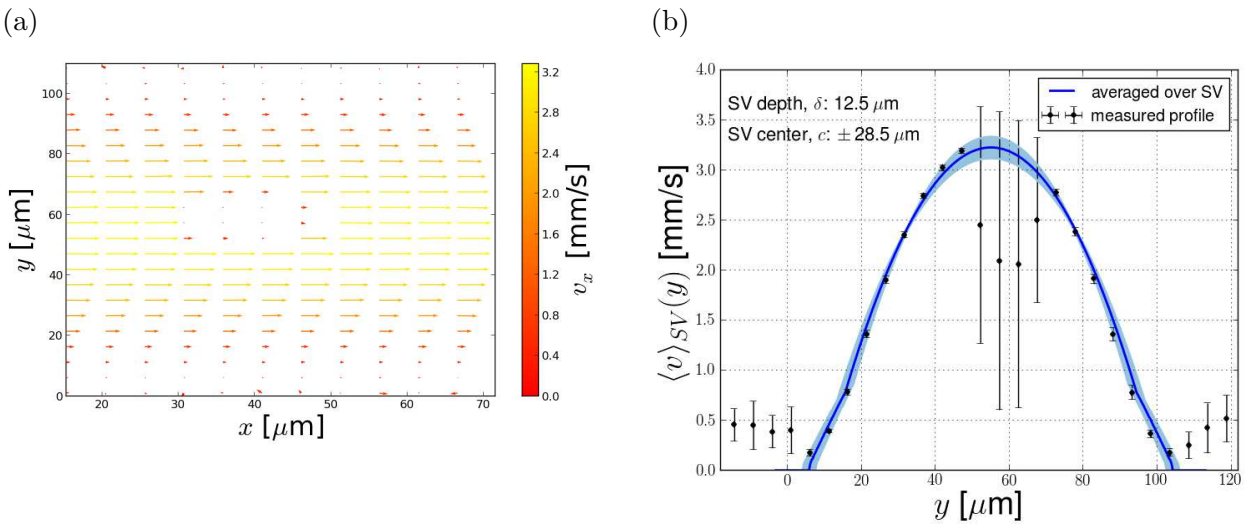

Figure 7: Flow profile for an experiment in which some of the velocity vectors could not be determined correctly. The pump rate for this experiment was 75 μl/h. (a) Measured flow field in which at least four of the profiles have incorrect velocities near the center of the channel. (b) Fit to the data, demonstrating the robustness of our method. The large error bars near the center of the profile result from the incorrect vectors.

6.3 Varying Experimental and Processing Parameters

In this section we show fits from a variety of other tests, from which can be seen how variables such as flow rate, focus, and processing options can affect the size, δ, and position, c, of the SV. We also discuss how the measured SV differs from the calculated DOC [20], and how the two have complimentary roles. As in Section 4, error bars represent one standard deviation in the set of all profiles measured along the x direction. The blue shaded area represents the combined uncertainty in the actual fluid flow, which results from our uncertainty in the channel cross section and the flow rate of the pump. Note that, to within our experimental uncertainties, a simple rectangular SV suffices to explain all of the results.

Figure 8 shows fits for two measurements on the same channel and for the same flow rate. The velocity field of the fluid within the channel is therefore the same for both measurements. The velocity profiles measured by μPIV differ, however, because, between the measurement in Figure 8(a) and the measurement in Figure 8(b), the pump was briefly disconnected from and then reconnected to the microchannel, and the microscope was refocused. All processing options were consistent between the two experiments. Though quality of focus is largely subjective, averaging over the SV can explain both measurements. In this case, refocusing changes the position of the SV but not its thickness.

In Figure 9 and Table 1 one can see the effects on the SV of differing processing options and flow rates. Figure 9 shows two measured results for the same experiment, in which the fluid injection rate was 100 μl/h. Both measured velocity profiles were obtained from

(a) (b)

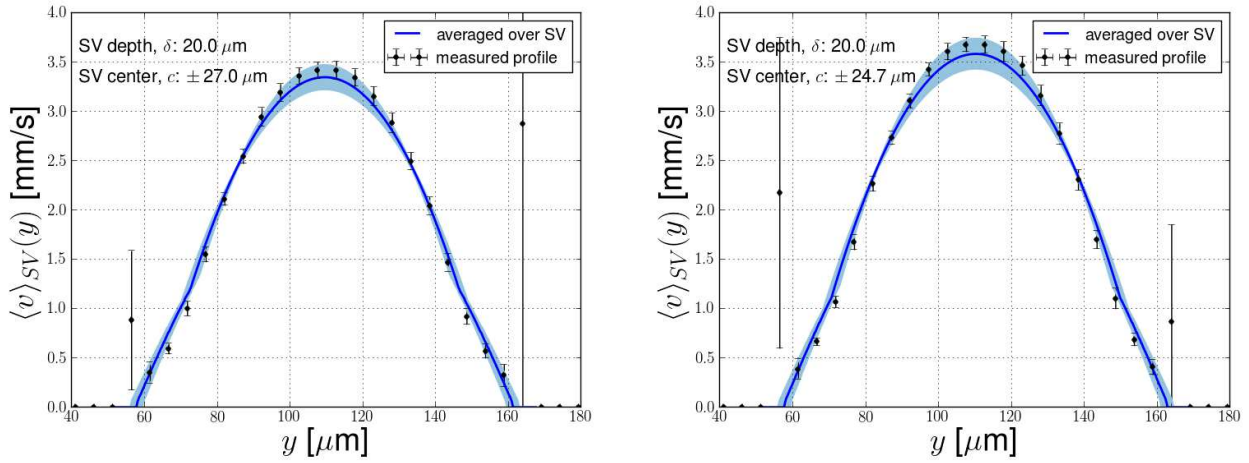

Figure 8: Fits to the experimental profiles obtained with fluid injection rate of 75 μl/h. (a) Before disconnecting from the pump and (b) after reconnecting to the pump and refocusing.

(a) (b)

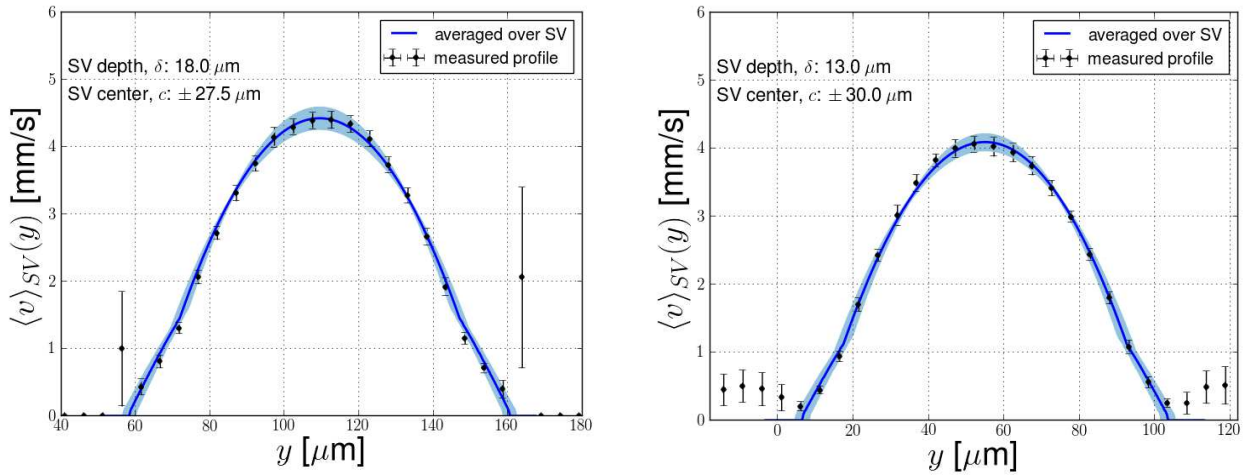

Figure 9: Flow profile obtained after processing the same set of CCD images with (a) Insight 3G and (b) OpenPIV software. The processing options are detailed in Section 3.3. Figure 9(a) is a reproduction of the fit shown in Figure 3. We have included it again here for easier comparison.

the same set of CCD images. They differ only in the image processing options, which are discussed in Section 3.3. The positions of the SV center, c, and the SV thickness, δ, resulting from the various processing options are listed in Table 1 for two fluid injection rates: $100\,\mu$l/h and $75\,\mu$l/h. For both flow rates, processing with OpenPIV results in a substantially thinner SV that is located slightly farther from the center of the channel. The preferred processing options may vary from case to case, and it is important to note that their effects on the SV can be quantified.

	Insight 3G	OpenPIV
$100\,\mu$l/h	$\delta = 18.0\,\mu$m	$\delta = 13.0\,\mu$m
	$c = \pm 27.5\,\mu$m	$c = \pm 30.0\,\mu$m
$75\,\mu$l/h	$\delta = 20.0\,\mu$m	$\delta = 12.5\,\mu$m
	$c = \pm 27.0\,\mu$m	$c = \pm 29.0\,\mu$m

Table 1: Comparison of the SV for two processing options and flow rates.

As discussed in Section 2.2, the DOC derived in [20] is often used as an estimate for the thickness of the SV, δ. We calculate the DOC for our experiments to be approximately $37\,\mu$m. This value is based on an assumed intensity threshold, ε, required for a particle image to affect significantly the processing. We have used the typical [15] value of $\varepsilon = 0.01$, which means we assume that contributions are made by out-of-focus particles with a minimum of 1% of the intensity of an in-focus particle. Note that this calculated value of the DOC is constant for all of our experiments presented in Sections 4 and 6, for which we have measured that the actual δ varies between $12.5\,\mu$m and $20\,\mu$m. The calculated DOC can be reconciled with the measured δ if one assumes that ε in fact varies between $\varepsilon = 0.245$ and $\varepsilon = 0.075$, but it is not clear how one could determine these thresholds without first measuring the SV for the various focus levels and processing options. While the DOC gives important intuition into the variables affecting δ, it does not replace a quantitatively determined SV.

6.4 Analysis of Scanning PIV

Kloosterman et al. [12] have recently claimed that a simple average, such as Equation (1), cannot explain the velocity measured by μPIV with a large depth of field. Rather than treat the entire profile from wall to wall, they have considered the difference between measured and predicted maximum speeds at the center of the microfluidic channel. In our Figure 3, for example, this corresponds to explaining why the maximum measured speed is approximately 4.4 mm/s (in symbols) rather than the theoretical maximum for a centered SV with zero thickness, 6.4 mm/s (dashed line).

Their claim is based on a common experimental procedure called "Scanning PIV", in which one systematically varies the location of the focal plane along the optical (z) axis and measures the velocity profile for each location. Their analysis is for Hagen-Poiseuille flow in a cylindrical channel, and because the maximum velocity in the channel occurs at its vertical center, the authors claim that from all the measured profiles from the scan, the

one with the highest peak velocity is the centered profile. Having centered the region over which particle images are resolved, then, they find that for large depths of field that cover the entire channel, the measured velocity is larger than what is predicted from averaging over the entire channel.

Using the average over the SV in Equation (1), however, we can show that this use of Scanning PIV will not find the center of the channel for large SV. To analyze the results published in Ref. [12], we use the Hagen-Poiseuille profile for flow in a cylindrical channel,

$$v_P(r) = v_0 \left(1 - \frac{r^2}{R^2}\right), \tag{7}$$

where v_0 is the maximum speed in the channel, r is the radial coordinate, R is the channel radius, and $r = 0$ at the center of the channel. Let us change to Cartesian coordinates with $z = 0$ at the vertical center of the channel, and substitute $D = 2R$ for the channel's diameter. In this section we are interested in the maximum speed, which occurs at the fixed y value of the center of the channel, $y = y_{\text{center}}$, while the SV changes. We will therefore fix y and emphasize the dependence of the speed on the position, c, and size, δ, of the SV. Let $\langle v \rangle_{SV}(y = y_{\text{center}}) \equiv \langle v \rangle_{SV}(c, \delta)$ denote our prediction of the maximum speed. Using Equation (1) with the Poiseuille profile (7), we find

$$\langle v \rangle_{SV}(c, \delta) = v_0 \left[1 - \frac{4}{3}\left(\frac{z_-^2 + z_- z_+ + z_+^2}{D^2}\right)\right], \tag{8}$$

where the dependence on c and δ is in the integration bounds $z_- = \text{Max}\,(c - \delta/2, -D/2)$ and $z_+ = \text{Min}\,(c + \delta/2, D/2)$, as before.

In terms of the notation in Equation (8), when one uses scanning PIV to find the center of a channel for a given δ, one varies c until $\langle v \rangle_{SV}(c, \delta)$ is maximized. The principal assumption, then, is that this maximum always occurs at $c = 0$. To check this assumption, we solve $\frac{\partial}{\partial c}\langle v \rangle_{SV}(c, \delta) = 0$ for c and find multiple solutions. One solution is for a centered SV, with $c = 0$, for which the maximum speed is

$$\langle v \rangle_{SV}(c, \delta)\Big|_{c=0} = \begin{cases} v_0 \left(1 - \frac{\delta^2}{3D^2}\right) & 0 \le \delta < D \\ \frac{2}{3} v_0 & \delta \ge D. \end{cases} \tag{9}$$

Another is for $c = \pm(D - 2\delta)/4$, for which the SV is not centered in the channel, and the maximum speed is

$$\langle v \rangle_{SV}(c, \delta)\Big|_{c=\pm(D-2\delta)/4} = \begin{cases} v_0 \frac{(9D^2 + 12D\delta - 16\delta^2)}{12D^2} & 0 \le \delta < \frac{3}{4} D \\ \frac{3}{4} v_0 & \delta \ge \frac{3}{4} D. \end{cases} \tag{10}$$

Figure 10 is a plot of $\langle v \rangle_{SV}(c, \delta)$ for these two maximizing values of c. The curves cross at $\delta = \frac{\sqrt{3}}{2} D$. Because the experimenter selects the value of c that maximizes the measured speed, for $\delta > \frac{\sqrt{3}}{2} D$ in a cylindrical channel, this scanning PIV method will position the SV

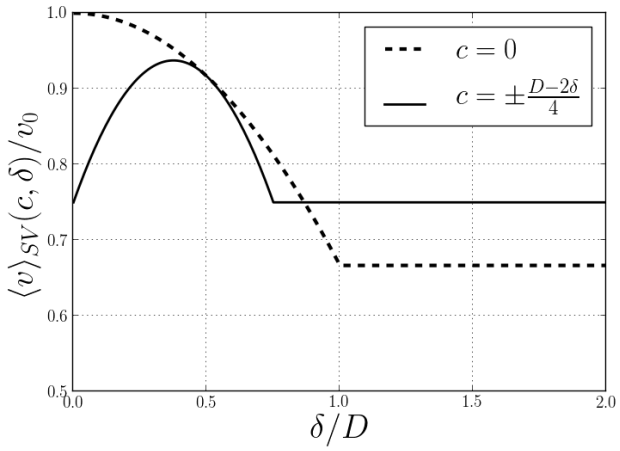

Figure 10: Maximum speed measured by the scanning PIV procedure as a function of δ. The dashed line is for a DOC centered at $c = 0$, while the solid line represents the maximum speed when the DOC is centered at $c = \pm(D - 2\delta)/4$.

away from the channel's center, at $c = \pm(D-2\delta)/4$. Thus, one must use Scanning PIV with caution.

Finally, we note that in Ref. [12] the authors base their claim on a method for calculating the simple average that is different from Equation (1). Because of the assumed ability of scanning PIV to locate the center of the cylindrical channel, they fix $c = 0$. Furthermore, they do not stop the integration at the bottom and top of the channel, and instead use $z_- = -DOC/2$ and $z_+ = +DOC/2$, where DOC is the Depth of Correlation we have discussed in Section 6.3. The result is

$$v_{\max}(DOC) = v_0 \left(1 - \frac{DOC^2}{3D^2}\right), \tag{11}$$

which has positive values only for $DOC/D < \sqrt{3}$. Though the DOC does not equal δ, the two can be roughly compared when both are as large as or larger than the channel diameter, D, and images cover the entire depth of the channel. In this case, the authors predict from Equation (11) that $v_{\max}(D) = \frac{2}{3}v_0$, but they measure $v_{\max}(D) \approx \frac{3}{4}v_0$ and find that it remains nearly constant for $DOC \gtrsim D$. We see from Figure 10 and Equation (10), however, that the simple average, combined with this use of Scanning PIV, does predict $\langle v \rangle_{SV}(c,\delta) = \frac{3}{4}v_0$ for large δ.

7 Conclusion

We show that a simple average over the Sampling Volume (SV) suffices to explain quantitatively the velocity profiles measured in μPIV experiments for which the depth of field has a size comparable to that of the microfluidics system itself. This allows rigorous verification

of the velocity fields of fluids flowing in microchannels. With this simple approach, one can easily understand and physically interpret the measured features of velocity profiles. In some cases, it allows the complete determination of an unknown flow rate or velocity field based only on the μPIV measurement. Furthermore, in a straightforward manner one can determine measurement uncertainty, which is essential for any quantitatively useful experiment. Because of the presence of a finite sampling region, in the past one has either ignored the magnitude of the measured velocity or else treated the effects of the finite volume as errors to be corrected by complicated processing.

By minimally processing data and retaining all measured features, such as kinks in the velocity profile, we have developed a method that is especially robust against noise and other common sources of measurement error. By comparing the measured velocity profiles to the theoretical predictions, we are able to quantify the effect on the SV of processing options and focus. We also provide a critical evaluation of Scanning PIV, which is often used to locate the center of a microchannel. We show how and why it in fact fails to locate the center for large SV. In general, the concept of the SV has implications for quantitative measurement of flow within channels on the micrometer scale and below.

Acknowledgments

We would like to thank Michael Engel from IBM Research – Watson as well as the LABNANO–CBPF for the SEM images, Diney Ether and the LPO–UFRJ for help with the calibration, Angelo Gobbi at the LMF–LNNano for profilometer measurements, and José Florián at PUC–Rio for help with the μPIV equipment.

References

[1] Stuart J Williams, Choongbae Park, and Steven T Wereley. Advances and applications on microfluidic velocimetry techniques. *Microfluid Nanofluid*, 8(6):709–726, 2010.

[2] Ralph Lindken, Massimiliano Rossi, Sebastian Große, and Jerry Westerweel. Micro-particle image velocimetry (μPIV): Recent developments, applications, and guidelines. *Lab Chip*, 9(17):2551–2567, 2009.

[3] Steven T Wereley and Carl D Meinhart. Recent advances in micro-particle image velocimetry. *Annu. Rev. Fluid Mech.*, 42:557–576, 2010.

[4] Ronald J Adrian and Jerry Westerweel. *Particle image velocimetry*, volume 30. Cambridge University Press, 2010.

[5] Eric K Sackmann, Anna L Fulton, and David J Beebe. The present and future role of microfluidics in biomedical research. *Nature*, 507(7491):181–189, 2014.

[6] Daniel Mark, Stefan Haeberle, Günter Roth, Felix von Stetten, and Roland Zengerle. Microfluidic lab-on-a-chip platforms: requirements, characteristics and applications. *Chem. Soc. Rev.*, 39(3):1153–1182, 2010.

[7] Naga Siva Kumar Gunda, Bijoyendra Bera, Nikolaos K Karadimitriou, Sushanta K Mitra, and S Majid Hassanizadeh. Reservoir-on-a-Chip (ROC): A new paradigm in reservoir engineering. *Lab Chip*, 11(22):3785–3792, 2011.

[8] Pierre Joseph and Patrick Tabeling. Direct measurement of the apparent slip length. *Phys. Rev. E*, 71(3):035303, 2005.

[9] Peichun Tsai, Alisia M Peters, Christophe Pirat, Matthias Wessling, Rob GH Lammertink, and Detlef Lohse. Quantifying effective slip length over micropatterned hydrophobic surfaces. *Phys. Fluids*, 21(11):112002, 2009.

[10] Carl D Meinhart, Steve T Wereley, and Juan G Santiago. PIV measurements of a microchannel flow. *Exp. Fluids*, 27(5):414–419, 1999.

[11] Kristin Sott, Tobias Gebäck, Maria Pihl, Niklas Lorén, Anne-Marie Hermansson, Alexei Heintz, and Anders Rasmuson. μPIV methodology using model systems for flow studies in heterogeneous biopolymer gel microstructures. *J. Colloid Interf. Sci.*, 398:262–269, 2013.

[12] A Kloosterman, C Poelma, and J Westerweel. Flow rate estimation in large depth-of-field micro-PIV. *Exp. Fluids*, 50(6):1587–1599, 2011.

[13] Massimiliano Rossi, Rodrigo Segura, Christian Cierpka, and Christian J Kähler. On the effect of particle image intensity and image preprocessing on the depth of correlation in micro-PIV. *Exp. Fluids*, 52(4):1063–1075, 2012.

[14] J Westerweel, PF Geelhoed, and R Lindken. Single-pixel resolution ensemble correlation for micro-PIV applications. *Exp. Fluids*, 37(3):375–384, 2004.

[15] C Cierpka and CJ Kähler. Particle imaging techniques for volumetric three-component (3d3c) velocity measurements in microfluidics. *J. Vis.*, 15(1):1–31, 2012.

[16] Boris Chayer, Katie L Pitts, Guy Cloutier, and Marianne Fenech. Velocity measurement accuracy in optical microhemodynamics: experiment and simulation. *Physiol. Meas.*, 33(10):1585, 2012.

[17] J Westerweel. Fundamentals of digital particle image velocimetry. *Meas. Sci. Technol.*, 8(12):1379, 1997.

[18] Lukas Novotny and Bert Hecht. *Principles of nano-optics*. Cambridge university press, 2012.

[19] CD Meinhart, ST Wereley, and MHB Gray. Volume illumination for two-dimensional particle image velocimetry. *Meas. Sci. Technol.*, 11(6):809, 2000.

[20] MG Olsen and RJ Adrian. Out-of-focus effects on particle image visibility and correlation in microscopic particle image velocimetry. *Exp. Fluids*, 29(1):S166–S174, 2000.

[21] CD Meinhart, AK Prasad, and RJ Adrian. A parallel digital processor system for particle image velocimetry. *Meas. Sci. Technol.*, 4(5):619, 1993.

[22] José Angel Florián Gutiérrez and Marcio S Carvalho. Flow of oil drops through micro-capillaries. In *22nd International Congress of Mechanical Engineering (COBEM 2013)*, pages 6458–6469, 2013.

[23] Zachary J Taylor, Roi Gurka, Gregory A Kopp, and Alex Liberzon. Long-duration time-resolved PIV to study unsteady aerodynamics. *Instrumentation and Measurement, IEEE Transactions on*, 59(12):3262–3269, 2010.

[24] Shiyi Chen and Gary D Doolen. Lattice boltzmann method for fluid flows. *Annu. Rev. Fluid Mech.*, 30(1):329–364, 1998.